Bulletin of the Seismological Society of America, Vol. 99, No. 6, pp. 3487–3495, December 2009, doi: 10.1785/0120090108

Ⓔ

Short Note

Temporal Changes in Site Response Associated with the Strong Ground Motion of the 2004 M_w 6.6 Mid-Niigata Earthquake Sequences in Japan

by Chunquan Wu, Zhigang Peng, and Dominic Assimaki

Abstract We analyzed temporal changes in site response associated with the strong ground motion of the 2004 M_w 6.6 Mid-Niigata earthquake sequence in Japan. The seismic data were recorded at a site with accelerometers at the surface and a 100-m-deep borehole. We computed the empirical surface-to-borehole spectral ratios and used them to track temporal changes in the top 100 m of the crust. We observed that the peak spectral ratio decreases by 40%–60% and the peak frequency drops by 30%–70% immediately after large earthquakes. The coseismic changes are followed by apparent recoveries, with the time scale ranging from several tens to more than 100 sec. The coseismic peak frequency drop, peak spectral ratio drop, and the postseismic recovery time roughly scale with the input ground motions when the peak ground velocity is larger than ~5 cm/sec (or the peak ground acceleration is larger than ~100 Gal). Our results suggest that at a given site the input ground motion plays an important role in controlling both the coseismic change and the postseismic recovery in site response.

Online Material: Table of event information and computed parameters.

Introduction

It has been long recognized that local site conditions have significant effects on the strong ground motions generated by large earthquakes (e.g., Joyner *et al.*, 1976; Chin and Aki, 1991; Yu *et al.*, 1992). These studies have illustrated that the dynamic material properties, such as the shear modulus (G) and material attenuation (ξ), control the amplitude and frequency content of ground motions. More specifically, because the seismic velocities and densities of shallow sediments are generally much lower than those of the bedrock, amplification and resonance effects would occur due to conservation of energy. When the amplitude of the incident wave exceeds a certain threshold, the sediment response does not follow the linear Hooke's law with the input ground motion, resulting in nonlinear site effects. Overall, nonlinear effects have been shown to strongly correlate with the level of ground motion (e.g., Hartzell, 1998; Su *et al.*, 1998; Johnson *et al.*, 2009) and local soil conditions (e.g., Beresnev and Wen, 1996; Hartzell, 1998; Tsuda *et al.*, 2006), and in terms of ground motion amplitude, typically manifest beyond an amplitude threshold of 100–200 Gal (Beresnev and Wen, 1996). An improved knowledge on nonlinear site response is critical for better understanding and predicting strong ground motions.

While most previous studies have focused on direct comparisons of site response during strong and weak ground motions to infer soil nonlinearity, several recent studies have also investigated the details of the nonlinearity recovery process by means of the spectral ratio method in different regions (e.g., Pavlenko and Irikura, 2002; Sawazaki *et al.*, 2006; Karabulut and Bouchon, 2007; Sawazaki *et al.*, 2009; Wu *et al.*, 2009). A general pattern that emerged from these studies is a sharp reduction (on the order of 20%–70%) of measured peak frequencies (i.e., resonant frequencies) in the spectral ratios during the strong ground motions of the nearby large mainshock, followed by a time-dependent logarithmic recovery to the level before the mainshock. However, the speed and time scale of the postseismic recovery is quite different, including near-instant recovery (Karabulut and Bouchon, 2007), a few to tens of minutes (Pavlenko and Irikura, 2002; Sawazaki *et al.*, 2006), around one day (Wu *et al.*, 2009), and several years (Sawazaki *et al.*, 2006, 2009). It is still not clear whether the wide range of recovery time scales observed in these studies are mainly caused by differences in the local site conditions, choice of the reference site, employed method, or other factors. Whether the input ground motion is among the

controlling parameters for the time scale or the speed of the postseismic recovery remains an open question.

A better understanding of the coseismic change and postseismic recovery in site response requires a good estimate of the input motion, and by far the best, although not perfect, source of information on the input motion came from downhole arrays. Downhole array records have provided direct *in situ* evidence of nonlinearity (e.g., Seed *et al.*, 1970; Satoh *et al.*, 2001). They are generally more accurate than surface-rock records as the input motion to surface soil (e.g., Satoh *et al.*, 1995; Steidl *et al.*, 1996), although the downgoing wave fields presented in borehole recordings could introduce some bias (Steidl *et al.*, 1996). In this study, we apply a spectral ratio method to the strong-motion data recorded by a pair of surface and borehole stations before, during, and after the 2004 Mid-Niigata earthquake sequence (Fig. 1). The M_w 6.6 mainshock was followed by a vigorous aftershock sequence with at least three ~M_w 6 events, which provides an ideal dataset to quantify the effects of the input ground motion on the degrees of nonlinearity and the recovery processes.

Data and Analysis Procedure

Seismic Data

The analysis employs strong-motion data recorded by station NIGH06 in the Japanese Digital Strong-Motion Seismograph Network KiK-net operated by National Research Institute for Earth Science and Disaster Prevention (Aoi *et al.*,

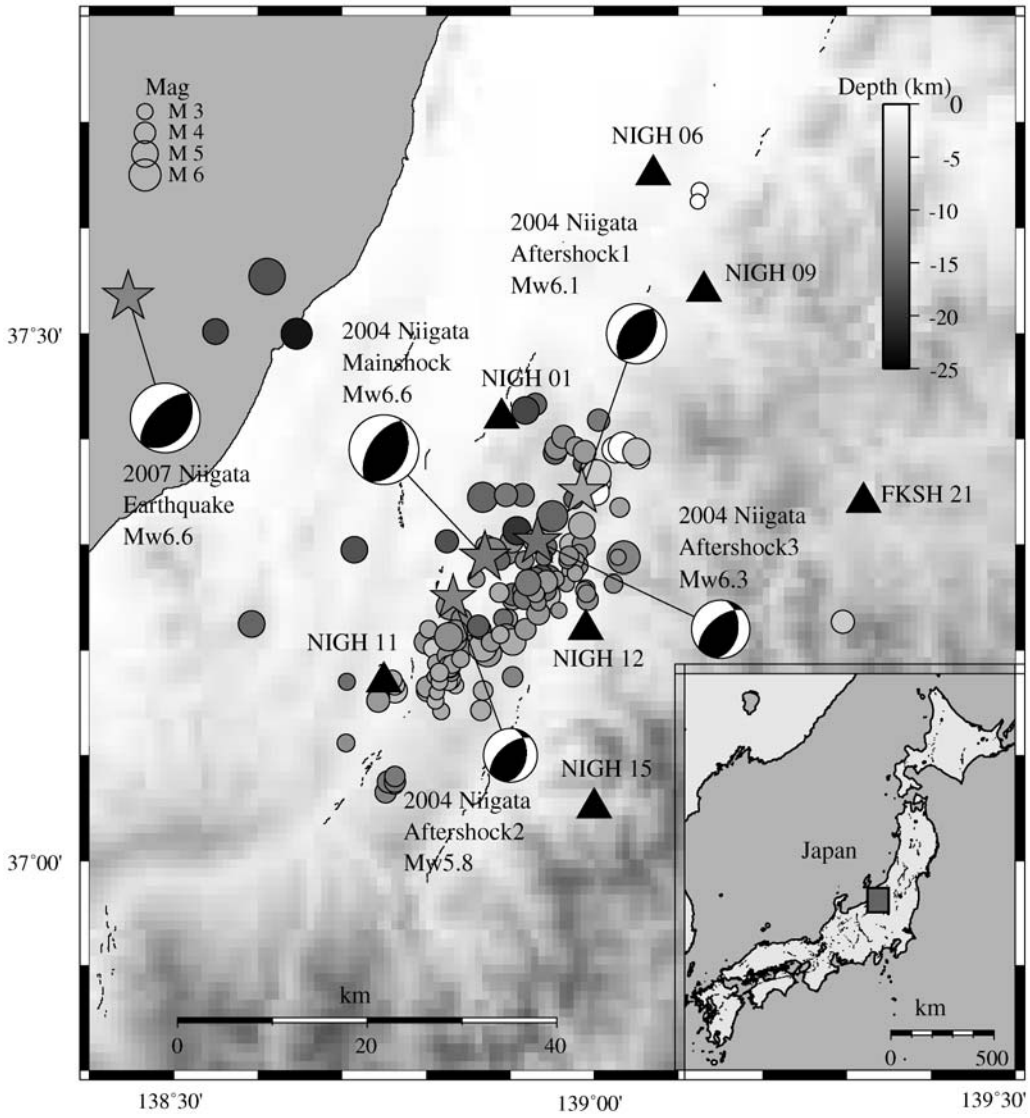

Figure 1. Topography map of the area along the west coast of Honshu, Japan. Shaded background indicates topography with white being low and dark being high. Epicenters of the 2004 M_w 6.6 Mid-Niigata mainshock, three large aftershocks, and the 2007 M_w 6.6 Niigata-ken Chuetsu-oki earthquake are shown as stars together with their moment tensor solution. Other events are shown as circles. The size of the circle indicates the magnitude of each event, and the gray scale shows the depth, with white being shallow and dark being deep. Locations of seven KiK-net stations within 50 km of the epicenter of the 2004 Mid-Niigata mainshock with PGA greater than 200 Gal are shown as black triangles. The black dash lines show the faults in this region. The inset shows a map of Japan. The box indicates the region shown in the topography map.

2000). The network consists of 659 stations with an uphole/downhole pair of strong-motion seismometers. Each KiK-net unit consists of three-component accelerometers and a data logger having a 24 bit analog-to-digital converter with a sampling frequency of 200 Hz.

Among all the eight stations within 50 km of the epicenter of the 23 October 2004 M_w 6.6 Mid-Niigata earthquake, the recorded peak ground acceleration (PGA) at stations NIGH01, NIGH06, NIGH09, NIGH11, NIGH12, NIGH15, and FKSH21 is larger than 200 Gal, a common threshold for nonlinear site amplification as found from previous studies (Chin and Aki, 1991; Beresnev and Wen, 1996). We focus on the station NIGH06 (see Fig. 1) for detailed analysis in this study mainly because the structure beneath the surface station is relatively simple with very low *S*-wave velocities, which has a larger potential for generating nonlinearity than other stations (Steidl *et al.*, 1996; Tsuda *et al.*, 2006). Indeed, the observed temporal changes in peak frequencies and peak spectral ratios (maximum of the spectral ratios) at station NIGH06 are much larger than those at other stations, allowing us to better quantify the differences associated with varying ground motions.

The borehole depth (below the surface) for station NIGH06 is 100 m. The rock types between the surface and borehole stations are clay with sand at the top 4 m, organic clay from 4 to 7 m, gravel from 7 to 43 m, and sandstone–mudstone from 43 to 100 m. For additional details regarding the network and site conditions see the Data and Resources section.

Analysis Procedure

The analysis procedure generally follows Sawazaki *et al.* (2006, 2009) and Wu *et al.* (2009) and is briefly described here. We use two horizontal-component accelerations recorded at the surface and borehole seismometers and generated by 235 earthquakes. These include 38 events starting 4 yrs before the Mid-Niigata mainshock and 196 events within 4 yrs after the mainshock. The magnitudes of most events (except the mainshock and some regional large events) range from 3 to 6.5, and the hypocentral depths range from 5 to 15 km (Ⓔ see the supplemental table available in the electronic edition of *BSSA*).

We analyze the entire seismic data using two slightly different approaches (Wu *et al.*, 2009). In the first approach, we use 10-sec time windows that are moved forward by 5 sec for all waveforms recorded by the surface and borehole stations. In this case all possible seismic phases, including pre-event noise, *P*, *S*, and coda waves, are analyzed together. This sliding-window-based approach is applied to the records of the Mid-Niigata mainshock and three largest aftershocks with magnitude $M_w > 6$ to track the temporal changes immediately after the strong motion and also to all the events for the statistical analysis described later in the Results section. In the second approach we only analyze data within a 10-sec-long coda-wave window, which starts from twice the direct *S*-wave travel time after the origin time of each event (Sawazaki *et al.*, 2006). Figure 2a shows an example of the original acceleration records generated by an *M* 5.2 aftershock on 4 November 2004 and the coda-wave window used to compute the spectral ratio. To avoid mixing coda waves with other phases, we did not use the records in the coda-window-based analysis if there are any other events between the onset of the *S* wave and the end of the coda window or if *S*-wave phases cannot be clearly identified. The coda-window-based approach has been shown to have less scatter than the sliding-window-based analysis (Sawazaki *et al.*, 2006; Wu *et al.*, 2009), and here we apply it to all the events to track possible long-term changes.

Next, we remove the mean value of the traces and apply a 5% Hanning taper to both ends. We add the power spectra of the two horizontal components and take the square root of the sum to get the amplitude of the vector sum of the two horizontal spectra. The obtained spectra are smoothed by applying the mean smoothing algorithm from the subroutine smooth in the seismic analysis code (Goldstein *et al.*, 2003), with a half-width of five points. The spectral ratio is obtained by taking the ratio of the horizontal spectra for surface and borehole stations. The amplitude of the spectra for both the surface and downhole recordings and the resulting spectral ratio for the aforementioned aftershock recordings are shown in Figure 2b and c.

Results

After processing all the data, we obtain 5935 spectral ratio traces for station NIGH06 from the sliding-window-based analysis. From the coda-window-based analysis, we obtain 210 spectral ratio traces. Next, we select those spectral ratio traces from events with a PGA exceeding 20 Gal to ensure signal-to-noise ratio, and combine the spectral ratios from the sliding-window-based analysis for the Mid-Niigata mainshock and largest aftershocks with those from the coda-window-based analysis for all the other selected events (Fig. 3). The running spectral ratios show clear decreases in peak spectral ratios and peak frequencies at the time of the mainshock and three large aftershocks, followed by a logarithmic-type recovery. In addition, the coseismic changes appear to be different for these events.

To better quantify the degree of coseismic change and the time scale of postseismic recovery, we stack the traces of NIGH06 in different time periods. We divide the selected dataset into the following periods: before the mainshock, every 0.25 in the logarithmic time after the mainshock and three largest aftershocks, and then every 0.5 in the logarithmic time for the following events. We have tested averaging the peaks using slightly different time windows, and the obtained results are similar. Logarithmic time is used instead of linear time because previous studies have always found a logarithmic recovery process for the observed temporal changes in the shallow crust (Rubinstein and Beroza, 2004; Schaff and Beroza, 2004; Rubinstein and Beroza, 2005; Li *et al.*,

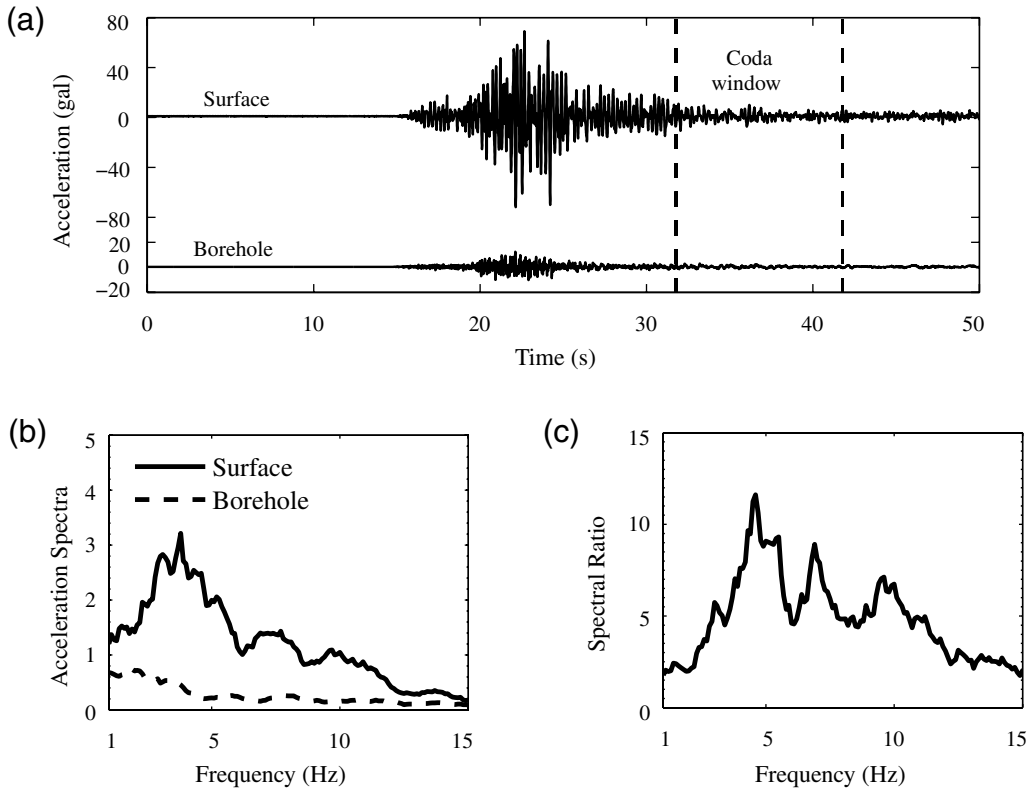

Figure 2. (a) East-component ground accelerations recorded at the station NIGH06 generated by an M 5.2 earthquake on 4 November 2004. The surface recording is shown at the top and the borehole recording is shown at the bottom of the panel. The dashed lines indicate the coda window that is used to compute (b) the acceleration spectra and (c) the spectral ratio.

2006; Peng and Ben-Zion, 2006; Sawazaki *et al.*, 2006; Rubinstein *et al.*, 2007, Sawazaki *et al.*, 2009; Wu *et al.*, 2009). Next, we identify the peak spectral ratio and peak frequency of the stacked trace in each period (Fig. 4). The obtained results again show a sudden drop of peak spectral ratio and a shift of the spectral peak to lower frequencies during each large event, followed by logarithmic recovery with a time scale of several tens to more than 100 sec.

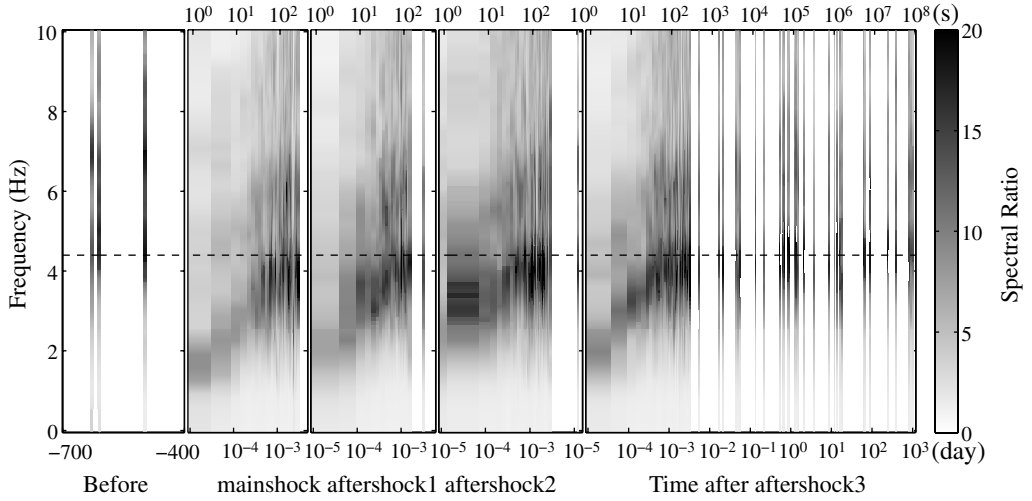

Figure 3. Temporal changes of the spectral ratio at station NIGH06 during the 2004 Mid-Niigata earthquake sequence. The left-hand bin shows the gray-scale-coded spectral ratios for events before the mainshock. The middle and right-hand bins show those for the mainshock and three aftershocks. Values shown on the top and bottom of the figure indicate the lapse times after the mainshock and large aftershocks in seconds and in days, respectively. Gaps represent no data. The horizontal black dashed line shows the value of the peak frequency before the mainshock.

Finally, we examine the relationship between the observed temporal changes and the input ground motion by comparing the percentage of drop in peak frequency, peak spectral ratio, time scale of recovery, and recovery speed with the PGA (Fig. 5) and peak ground velocity (PGV) (Fig. 6) for each event. The PGA and PGV for each event are measured from the amplitude of the vector sum of the two horizontal-component ground acceleration and velocity records, respectively. The ground velocity records are obtained by integrating the original acceleration records and then applying a 1–20 Hz Butterworth band-pass filter to remove the shift in the direct-current component. We use the averaged peak frequency and peak spectral ratio from coda-window-based spectral ratios of the 56 events before the 2004 Mid-Niigata mainshock as the reference values. We first calculate the percentage in coseismic reduction for both peak spectral ratio and peak frequency by comparing the 10-sec windows immediately after the direct *S*-wave arrivals with the reference values. The recovery time is identified when the values from the sliding 10-sec windows are recovered to 90% of the reference values. The apparent recovery speed is simply the ratio between the coseismic drop and the recovery time. As shown in Figures 5 and 6, the coseismic peak frequency, peak spectral ratio drop, and the postseismic recovery times roughly scale with the input ground motion when the PGV is larger than 5 cm/sec (or PGA is larger than 100 Gal). When the input ground motion is relatively small, the measurements are scattered and do not show a clear relationship with either PGV or PGA. For the events with PGV larger than 5 cm/sec (or PGA larger than 100 Gal), we also apply a slightly different technique by applying least-squares fitting to the sliding-window measurement to obtain the recovery speed first, and then calculating the coseismic drop and recovery time from the recovery speed. We did not apply the least-squares fitting to the measurements with PGV less than 5 cm/sec (or PGA less than 100 Gal) due to a lack of enough data points below the reference values. The obtained recovery times from the least-squares fitting for events with larger input motions are slightly higher than the previous method, but the general trend with the PGV or PGA remains essentially the same.

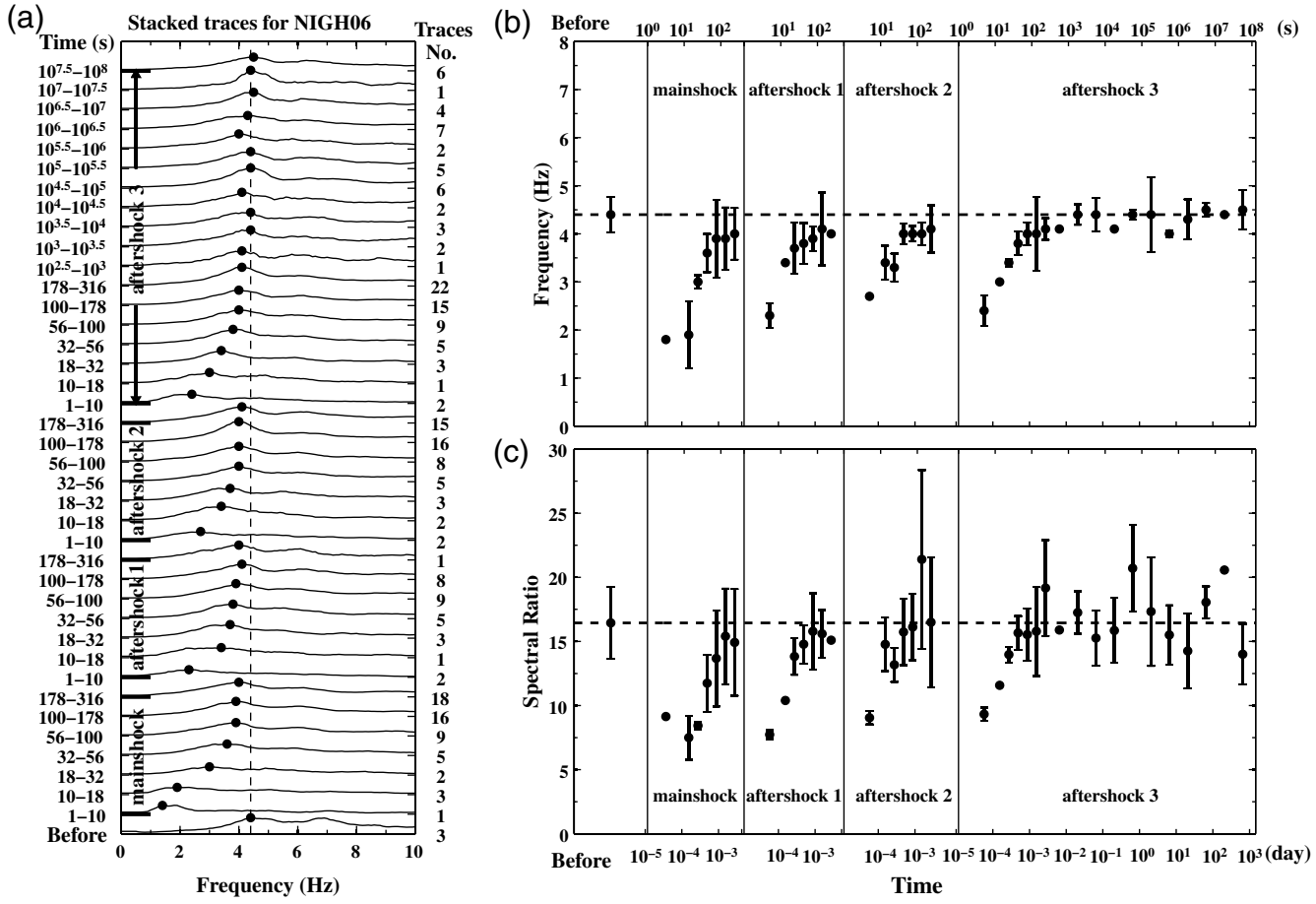

Figure 4. (a) Spectral ratios stacked within different time periods at station NIGH06 during the 2004 M_w 6.6 Mid-Niigata earthquake sequence. The solid circle marks the peak spectral value, and the dashed line marks the peak frequency level before the mainshock. The time windows and number of traces used to generate each stack are marked on the left- and right-hand side, respectively. (b) Peak frequency and (c) peak spectral ratio measured from the stacked spectral ratio traces in (a) before and after the mainshock. The vertical solid bar centered at each data point shows the standard deviation. The dashed line indicates the value before the mainshock.

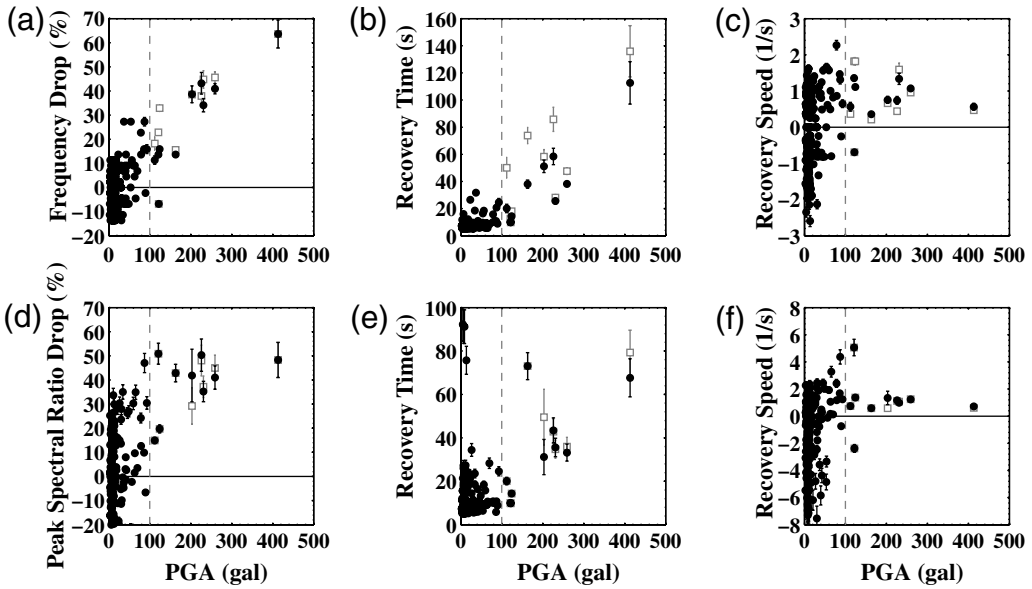

Figure 5. (a) Percentage drop of the peak frequency plotted against the PGA at NIGH06 for all 235 events. The solid circles mark the values measured from the 10-sec windows immediately after the direct *S*-wave arrivals. The open squares show the values calculated from least-squares fitting of the sliding-window measurements for events with PGA larger than 100 Gal. The vertical solid bar centered at each data point shows the standard deviation. The horizontal black solid line indicates the value before the mainshock. The vertical gray dashed line marks the PGA value of 100 Gal. (b) Recovery time to the reference peak frequency versus the PGA. (c) Apparent recovery speed of the peak frequency versus the PGA. (d) Percentage drop of the peak spectral ratio versus the PGA. (e) Recovery time to the reference peak spectral ratio versus the PGA. (f) Apparent recovery speed of the peak spectral ratio versus the PGA.

Discussion

The ground motion recorded at surface stations is a convolution of the source, path, and site effects. The temporal changes of the spectral ratios observed in this study could be caused by changes in the seismic source spectrum, apparent changes produced by varying source locations, and physical changes occurring during the propagation path and in shallow sediments. As shown in Figure 1, the station NIGH06 is not right on top of the aftershock zone. However, because the surface and borehole stations are very close to each other (100 m) as compared to the distances between the

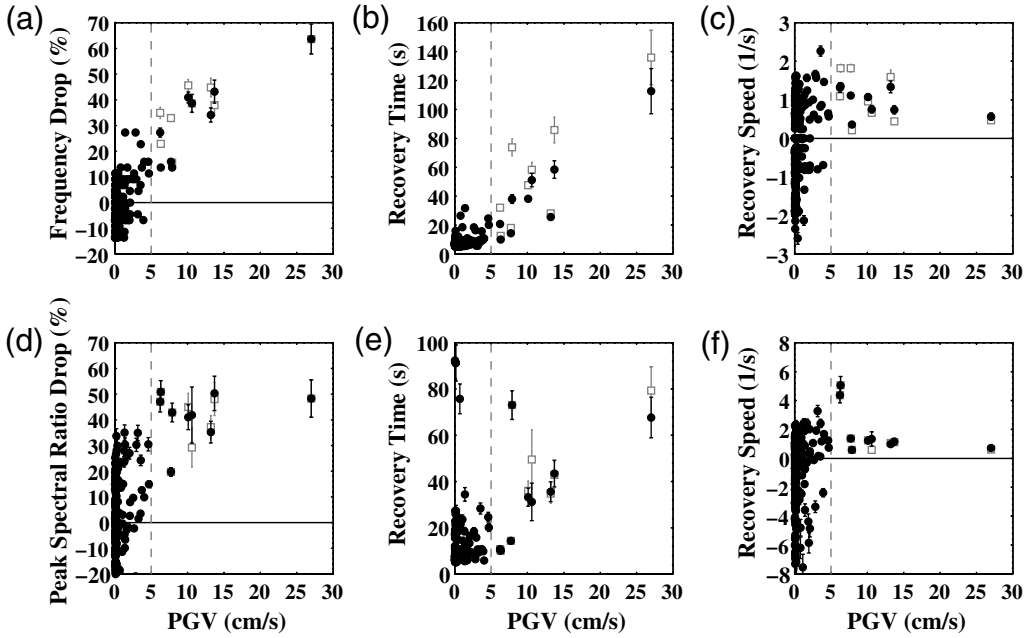

Figure 6. Similar plots as Figure 5 using PGV as the *x*-axis. The vertical gray dashed line marks the PGV value of 5 cm/sec.

earthquake sources and stations (typically more than 10 km), the seismic sources and the propagation path are almost identical for the colocated surface and borehole stations. Hence, apparent changes from variable source locations and propagation paths are unlikely to be the main cause of the observed temporal changes.

Temporal changes of material properties within the surface soil layer induced by the strong ground motion of the large earthquakes are likely to be the main origin of the observed variations in the spectral ratios and peak frequencies. The sharp reductions in the spectral ratios and peak frequencies are usually considered as two signatures of *in situ* nonlinear site response during strong shaking (e.g., Field *et al.*, 1997; Beresnev *et al.*, 1998), which corresponds to a reduction in soil strength and an increase in soil damping observed during earlier laboratory studies (e.g., Seed *et al.*, 1969, 1970).

Assuming a soft soil layer over a half-space bedrock with large impedance contrast (Dobry *et al.*, 2000), the fundamental resonant frequency f of the soil layer can be computed by

$$f = \frac{V_S}{4H} = \frac{\sqrt{G/\rho_s}}{4H}, \tag{1}$$

where V_S, H, G, and ρ_s are the S-wave velocity, thickness, shear modulus, and density of the surface soil layer, respectively. According to the NIGH06 site profile provided by KiK-net, the top two layers are clay with sand from 0 to 4 m and organic clay from 4 to 10 m, both with very low S-wave velocities of 100–270 m/sec, as compared with the 740 m/sec below 10 m. Hence, the previous assumption is justified. In addition, the fundamental frequency observed from spectral ratios before the 2004 Mid-Niigata earthquake is ~4.4 Hz, which agrees well with the resonance frequency (4 Hz) of the top two layers (i.e., $H = 10$ m). Hence, we infer that the resonance effect and observed temporal variations in the peak frequencies are mainly constrained in the top 10 m of near-surface layers.

Similarly, the amplification factor (AMP), impedance contrast (I), and damping ratio (ξ) follow the relation (Dobry *et al.*, 2000)

$$\mathrm{AMP} = \frac{2}{(1/I) + (\pi/2)\xi}. \tag{2}$$

With the assumption of large impedance contrast, the term $1/I$ could be ignored and equation (2) could be simplified as

$$\mathrm{AMP} = \frac{4}{\pi\xi}. \tag{3}$$

Finally, we compute the dynamic strain γ as (e.g., Hill *et al.*, 1993)

$$\gamma = \frac{\mathrm{PGV}}{V_S}. \tag{4}$$

Using equations (1)–(4), we can relate the observed temporal changes in the peak frequency and peak spectral ratios to changes in the shear modulus G and the material damping ξ, as well as the dynamic strain γ.

The relationship between G/G_0, ξ, and γ is shown in Figure 7, where G_0 is the average shear modulus measured before 2004 Mid-Niigata earthquake. Although we do not have measurements with higher strains ($\gamma > 0.004$), the modulus degradation and damping ratio curves generally follow typical values for generic clay sites (Vucetic and Dobry, 1991; Electric Power Research Institute [EPRI], 1993). As mentioned before, the degree of soil nonlinearity depends both on the material properties and the ground-motion characteristics, namely the amplitude and frequency content (e.g., Hartzell, 1998; Assimaki *et al.*, 2008). Although strong shaking causes physical changes and temporal variations of the material properties under the NIGH06 site, the event intervals are well beyond the maximum recovery time of ~150 sec (Fig. 6b). Hence, the material properties at site NIGH06 are almost recovered to the level before the mainshock when the next event occurs and could be considered as near identical for all the events analyzed in this study. Therefore, assuming that the site conditions are practically identical for all events investigated, we suggest that the observed variation in the degree of nonlinearity for the Mid-Niigata mainshock and aftershocks is likely caused by variations in the amplitude and/or frequency content of the input ground motions.

In this study, we found that the coseismic peak frequency drops, peak spectral ratio drops, and the postseismic recovery time increases as the PGV increases from ~5 cm/sec or the PGA increases from ~100 Gal. Our observations are generally consistent with the 100–200 Gal PGA

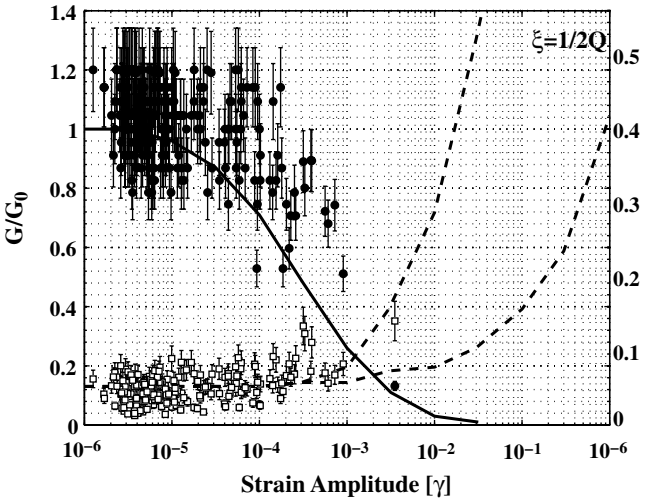

Figure 7. Calculated values of modulus degradation G/G_0 (solid circles) and damping ratio ξ (open squares) plotted against the dynamic strains (γ). The vertical solid bar centered at each data point shows the standard deviation. The left- and right-hand vertical axes correspond to the values of G/G_0 and ξ, respectively. The solid and dashed lines show the modulus reduction curve for clay (Vucetic and Dobry, 1991) and the typical range of damping ratio for clay (EPRI, 1993), respectively.

threshold for soil nonlinearity inferred from previous studies (e.g., Beresnev and Wen, 1996), indicating that input ground motion at a given site plays an important role in controlling the degree of the soil nonlinearity and the recovery process. However, nonlinear effects have been identified in laboratory studies of geomaterials under strains as low as 10^{-8} (TenCate *et al.*, 2004) and also *in situ* for a site under PGA of ~35 Gal (J. Rubinstein, unpublished manuscript, 2009). We note that the resolution of the recovery time in this study is somewhat limited by the 10-sec window, so the subtle nonlinearity and recovery associated with small events (i.e., PGA less than 100 Gal) could be buried under the averaging effects. Reducing the sliding-window size to smaller values would help to detect the subtle nonlinear site response associated with smaller input ground motions (e.g., J. Rubinstein, unpublished manuscript, 2009).

Recently Lyakhovsky *et al.* (2009) performed theoretical analyses and numerical simulations of the systematic shift of resonance frequencies based on the nonlinear continuum damage model. They found that under a constant material damage, the shift of the resonance frequency with increasing ground motion is only a few percent. However, for increasing material damage, the resonance frequency shift may reach to tens of percent. Here we observed large changes (30%–70%) in peak frequencies associated with the strong ground motions of the Mid-Niigata mainshock and its large aftershocks. Such a large change in the peak (resonance) frequencies suggests that the increasing ground motion with a constant level of damage itself cannot explain the observed features alone, and an increasing material damage in the near-surface layer is needed. This is also consistent with the observations that soft and unconsolidated near-surface sediments are more susceptible to damages caused by strong shaking, resulting in nonlinear site effects and postseismic recoveries (e.g., Rubinstein and Beroza, 2005; Sawazaki *et al.*, 2009). We note that the maximum time scale of recovery in this study is around 150 sec, which also corresponds to the maximum PGV observed during the Mid-Niigata mainshock. However, such a time scale is still several orders of magnitudes smaller than those measured at other KiK-net sites in Japan (Sawazaki *et al.*, 2006, 2009) and along the North Anatolian fault in Turkey (Wu *et al.*, 2009), indicating that different site conditions may cause a larger variability (at least in the postseismic recovery) than the input ground motion at a given site.

So far the mechanisms and the controlling parameters for temporal changes in the near-surface layers and the time scale of recovery are still under investigation. Logarithmic recovery of material damage has been observed by previous studies (e.g., Schaff and Beroza, 2004; Peng and Ben-Zion, 2006; Sawazaki *et al.*, 2006; Wu *et al.*, 2009), and fluid diffusion is suggested to play an important role in the recovery process. Although there is no direct evidence, if the assumption of fluid diffusion holds in our case, the recovery rate would be mainly controlled by the permeability of the site, which could also be associated with amplitude of seismic waves (e.g., Rubinstein and Beroza, 2005; Elkhoury *et al.*, 2006). On the other hand, laboratory studies also found logarithmic recovery under normal stress due to increasing contact area of crack surfaces or grains for geomaterial and sedimentary rocks (Marone, 1998; Vakhnenko *et al.*, 2005). Because we did not observe a clear relationship between apparent recovery speed and PGV (Fig. 6c and f), it is likely that the recovery process is much more complicated than a simple process that is solely controlled by the input ground motion. To clarify the physical processes of the recovery, *in situ* measurements of the pore pressures are necessary, and seismic inversion of time- and depth-dependent site properties would also be very helpful (Assimaki *et al.*, 2008; Sawazaki *et al.*, 2009).

Data and Resources

Seismograms used in this study were collected by the Japanese Digital Strong-Motion Seismograph Network KiK-net. Data can be obtained from the KiK-net Web site http://www.kik.bosai.go.jp/kik/index_en.shtml (last accessed August 2008), which also contains additional details regarding the network and site conditions.

Acknowledgments

We thank the National Research Institute for Earth Science and Disaster Prevention (NIED) for providing us with the strong-motion records of KiK-net. We thank Reiji Kobayashi for providing the knet2sac program to convert original K-NET data format into SAC format and Wei Li for helping with the data download and insightful discussions. The manuscript benefited from valuable comments by Justin Rubinstein, an anonymous referee, and Associate Editor Diane Doser. The study was funded by the National Science Foundation (Grant EAR-0710959).

References

Aoi, S., K. Obara, S. Hori, K. Kasahara, and Y. Okada (2000). New Japanese uphole/downhole strong-motion observation network: KiK-net, *Seism. Res. Lett* **72,** 239.

Assimaki, D., W. Li, J. Steidl, and K. Tsuda (2008). Site amplification and attenuation via downhole array seismogram inversion: A comparative study of the 2003 Miyagi-Oki aftershock sequence, *Bull. Seismol. Soc. Am.* **98,** no. 1, 301–330.

Beresnev, I., and K. Wen (1996). Nonlinear soil response—A reality?, *Bull. Seismol. Soc. Am.* **86,** no. 6, 1964–1978.

Beresnev, I., G. Atkinson, P. Johnson, and E. Field (1998). Stochastic finite-fault modeling of ground motions from the 1994 Northridge, California, earthquake. II. Widespread nonlinear response at soil sites, *Bull. Seismol. Soc. Am.* **88,** no. 6, 1402–1410.

Chin, B., and K. Aki (1991). Simultaneous study of the source, path, and site effects on strong ground motion during the 1989 Loma Prieta earthquake: A preliminary result on pervasive nonlinear site effects, *Bull. Seismol. Soc. Am.* **81,** no. 5, 1859–1884.

Dobry, R., R. Borcherdt, C. Crouse, I. Idriss, W. Joyner, G. Martin, M. Power, E. Rinne, and R. Seed (2000). New site coefficients and site classification system used in recent building seismic code provisions, *Earthq. Spectra* **16,** no. 41, 41–67.

Electric Power Research Institute (EPRI) (1993). Guidelines for determining design basis ground motions, *Electric Power Research Institute Technical Report*, EPRI TR-102293.

Elkhoury, J., E. Brodsky, and D. Agnew (2006). Seismic waves increase permeability, *Nature* **441,** no. 7097, 1135–1138.

Field, E. H., P. A. Johnson, I. A. Beresnev, and Y. H. Zeng (1997). Nonlinear ground-motion amplification by sediments during the 1994 Northridge earthquake, *Nature* **390,** no. 6660, 599–602.

Goldstein, P., D. Dodge, M. Firpo, and L. Minner (2003). SAC2000: Signal processing and analysis tools for seismologists and engineers, in *The IASPEI International Handbook of Earthquake and Engineering Seismology*, W. H. K. Lee, H. Kanamori, P. C. Jennings, and C. Kisslinger (Editors), Part B, Ch. 85.5, Academic Press, London.

Hartzell, S. (1998). Variability in nonlinear sediment response during the 1994 Northridge, California, earthquake, *Bull. Seismol. Soc. Am.* **88,** no. 6, 1426–1437.

Hill, D., P. Reasenberg, A. Michael, W. Arabaz, G. Beroza, D. Brumbaugh, J. Brune, R. Castro, S. Davis, and D. DePolo (1993). Seismicity remotely triggered by the magnitude 7.3 Landers, California, earthquake, *Science* **260,** no. 5114, 1617–1623.

Johnson, P., P. Bodin, J. Gomberg, F. Pearce, Z. Lawrence, and F. Menq (2009). Inducing *in situ*, nonlinear soil response applying an active source, *J. Geophys. Res.* **114,** no. B5, B05304.

Joyner, W., R. Warrick, and A. Oliver (1976). Analysis of seismograms from a downhole array in sediments near San Francisco Bay, *Bull. Seismol. Soc. Am.* **66,** no. 3, 937–958.

Karabulut, H., and M. Bouchon (2007). Spatial variability and non-linearity of strong ground motion near a fault, *Geophys. J. Int.* **170,** no. 1, 262–274.

Li, Y., P. Chen, E. Cochran, J. Vidale, and T. Burdette (2006). Seismic evidence for rock damage and healing on the San Andreas fault associated with the 2004 *M* 6.0 Parkfield earthquake, *Bull. Seismol. Soc. Am.* **96,** no. 4B, 349–363.

Lyakhovsky, V., Y. Hamiel, J. Ampuero, and Y. Ben-Zion (2009). Non-linear damage rheology and wave resonance in rocks, *Geophys. J. Int.* **178,** no. 2, 910–920, doi 10.1111/j.1365-246X.2009.04205.x.

Marone, C. (1998). Laboratory-derived friction laws and their application to seismic faulting, *Annu. Rev. Earth Planet. Sci.* **26,** no. 1, 643–696.

Pavlenko, O., and K. Irikura (2002). Nonlinearity in the response of soils in the 1995 Kobe earthquake in vertical components of records, *Soil. Dyn. Earthq. Eng.* **22,** no. 9–12, 967–975.

Peng, Z., and Y. Ben-Zion (2006). Temporal changes of shallow seismic velocity around the Karadere–Düzce branch of the North Anatolian fault and strong ground motion, *Pure Appl. Geophys.* **163,** no. 2, 567–600.

Rubinstein, J., and G. Beroza (2004). Evidence for widespread nonlinear strong ground motion in the M_w 6.9 Loma Prieta earthquake, *Bull. Seismol. Soc. Am.* **94,** no. 5, 1595–1608.

Rubinstein, J., and G. Beroza (2005). Depth constraints on nonlinear strong ground motion from the 2004 Parkfield earthquake, *Geophys. Res. Lett.* **32,** L14313.

Rubinstein, J., N. Uchida, and G. Beroza (2007). Seismic velocity reductions caused by the 2003 Tokachi-Oki earthquake, *J. Geophys. Res.* **112,** B05315.

Satoh, T., M. Fushimi, and Y. Tatsumi (2001). Inversion of strain-dependent nonlinear characteristics of soils using weak and strong motions observed by borehole sites in Japan, *Bull. Seismol. Soc. Am.* **91,** no. 2, 365–380.

Satoh, T., T. Sato, and H. Kawase (1995). Nonlinear behavior of soil sediments identified by using borehole records observed at the Ashigra Valley, Japan, *Bull. Seismol. Soc. Am.* **85,** no. 6, 1821–1834.

Sawazaki, K., H. Sato, H. Nakahara, and T. Nishimura (2006). Temporal change in site response caused by earthquake strong motion as revealed from coda spectral ratio measurement, *Geophys. Res. Lett.* **33,** no. 21, L21303, doi 21310.21029/22006GL027938.

Sawazaki, K., H. Sato, H. Nakahara, and T. Nishimura (2009). Time-lapse changes of seismic velocity in the shallow ground caused by strong ground motion shock of the 2000 Western-Tottori earthquake, Japan, as revealed from coda deconvolution analysis, *Bull. Seismol. Soc. Am.* **99,** no. 1, 352–366.

Schaff, D., and G. Beroza (2004). Coseismic and postseismic velocity changes measured by repeating earthquakes, *J. Geophys. Res.* **109,** B10302.

Seed, H., I. Idriss, and E. E. R. Center (1970). *Soil Moduli and Damping Factors for Dynamic Response Analyses*, College of Engineering, University of California.

Seed, H., I. Idriss, and G. E. Group (1969). *Influence of Soil Conditions on Ground Motions During Earthquakes*, University of California, Institute of Transportation and Traffic Engineering, Soil Mechanics Laboratory.

Steidl, J., A. Tumarkin, and R. Archuleta (1996). What is a reference site?, *Bull. Seismol. Soc. Am.* **86,** no. 6, 1733–1748.

Su, F., J. Anderson, and Y. Zeng (1998). Study of weak and strong ground motion including nonlinearity from the Northridge, California, earthquake sequence, *Bull. Seismol. Soc. Am.* **88,** no. 6, 1411–1425.

TenCate, J., D. Pasqualini, S. Habib, K. Heitmann, D. Higdon, and P. Johnson (2004). Nonlinear and nonequilibrium dynamics in geomaterials, *Phys. Rev. Lett.* **93,** no. 6, 065501, doi 10.1103/PhysRevLett.93.065501.

Tsuda, K., R. Archuleta, and S. Jamison (2006). Confirmation of nonlinear site response: Case study from 2003 and 2005 Miyagi-Oki earthquakes, *Bull. Seismol. Soc. Am.* **96,** no. 3, 926–942.

Vakhnenko, O., V. Vakhnenko, and T. Shankland (2005). Soft-ratchet modeling of end-point memory in the nonlinear resonant response of sedimentary rocks, *Phys. Rev. B* **71,** no. 174103, 1–14.

Vucetic, M., and R. Dobry (1991). Effect of soil plasticity on cyclic response, *J. Geotech. Eng.* **117,** no. 1, 89–107.

Wu, C., Z. Peng, and Y. Ben-Zion (2009). Non-linearity and temporal changes of fault zone site response associated with strong ground motion, *Geophys. J. Int.* **176,** no. 3, 265–278.

Yu, G., J. Anderson, and R. Siddharthan (1992). On the characteristics of nonlinear soil response, *Bull. Seismol. Soc. Am.* **83,** no. 1, 218–244.

School of Earth and Atmospheric Sciences
Georgia Institute of Technology
Atlanta, Georgia 30332
chunquanwu@gatech.edu
(C.W., Z.P.)

School of Civil and Environmental Engineering
Georgia Institute of Technology
Atlanta, Georgia 30332
(D.A.)

Manuscript received 30 April 2009